Minimal recipes for planetary cloudiness

George Datseris[1,1], Joaquin Blanco[2,2], Or Hadas[3,3], Sadrine Bony[4,4], Rodrigo Caballero[2,2], Yohai Kaspi[3,3], and Bjorn Stevens[5,5]

[1]Max Planck Institute for Meteorology
[2]Stockholm University
[3]Weizmann Institute of Science
[4]Sorbonne University
[5]Max Plank Institute for Meteorology

November 30, 2022

Abstract

Clouds are primary modulators of Earth's energy balance. It is thus important to understand the links connecting variabilities in cloudiness to variabilities in other state variables of the climate system, and also describe how these links would change in a changing climate. A conceptual model of global cloudiness can help elucidate these points. In this work we derive simple representations of cloudiness, that can be useful in creating a theory of global cloudiness. These representations illustrate how both spatial and temporal variability of cloudiness can be expressed in terms of basic state variables. Specifically, cloud albedo is captured by a nonlinear combination of pressure velocity and a measure of the low-level stability, and cloud longwave effect is captured by surface temperature, pressure velocity, and standard deviation of pressure velocity. We conclude with a short discussion on the usefulness of this work in the context of global warming response studies.

Minimal recipes for global cloudiness

George Datseris[1], Joaquin Blanco[2], Or Hadas[3], Sadrine Bony[4], Rodrigo Caballero[2], Yohai Kaspi[3], Bjorn Stevens[4]

[1]Max Planck Institute for Meteorology, Hamburg, Germany
[2]Department of Meteorology, Stockholm University, Stockholm, Sweden
[3]Department of Earth and Planetary Sciences, Weizmann Institute of Science, Rehovot, Israel
[4]Sorbonne University, LMD/IPSL, CNRS, Paris, France

Key Points:

- Model fits are performed to the spatiotemporal observed cloudiness over all oceans, using a minimal set of predictors and parameters
- Models capture global-mean, spatial variability, and mean seasonal cycle of long and shortwave cloud radiative effects
- Cloud albedo and longwave effect are captured by pressure velocity and its variance, surface temperature, and lower tropospheric stability

Corresponding author: George Datseris, `george.datseris@mpimet.mpg.de`

Abstract

Clouds are primary modulators of Earth's energy balance. It is thus important to understand the links connecting variabilities in cloudiness to variabilities in other state variables of the climate system, and also describe how these links would change in a changing climate. A conceptual model of global cloudiness can help elucidate these points. In this work we derive simple representations of cloudiness, that can be useful in creating a theory of global cloudiness. These representations illustrate how both spatial and temporal variability of cloudiness can be expressed in terms of basic state variables. Specifically, cloud albedo is captured by a nonlinear combination of pressure velocity and a measure of the low-level stability, and cloud longwave effect is captured by surface temperature, pressure velocity, and standard deviation of pressure velocity. We conclude with a short discussion on the usefulness of this work in the context of global warming response studies.

Plain Language Summary

Clouds are important for Earth's climate, because they affect a large portion of the planet's energy balance, and hence its mean temperature. To better understand how the interplay between cloudiness and energy balance would change in a changing climate, we need a better theoretical understanding of how many clouds are distributed over the planet, and how this connects with the state variables of the climate system such as temperature and wind speed. As our theoretical understanding is currently limited, in this work we illustrate the simplest way one could represent the spatiotemporal distribution of clouds over the whole planet. We believe that these simple representations will pave the way for a conceptual theory of global cloudiness and its impact on the energy balance. We show that the impact of cloudiness on both solar and terrestrial radiation balance can be captured well with only a few predictive fields, like surface temperature or vertical wind speed, combined simply and using only three tunable parameters.

1 Introduction

Clouds are one of the most fascinating, important, and complex components of Earth's climate system (Siebesma et al., 2020). Despite their importance, we lack theoretical understanding of what controls planetary-wide cloudiness. For example, while we have a good understanding of the microphysics of cloud generation and radiative transfer through clouds (Houze, 2014; Cotton et al., 2014; Siebesma et al., 2020), it is difficult to use these theories to make claims about global cloudiness. Earth System Models (ESMs) and other bottom-up approaches do couple cloud formation to the global circulation. However, so far they have not been proven effective in constraining global cloudiness variability (Sherwood et al., 2020; Zelinka et al., 2020). This makes it difficult to transparently establish links between variability in global cloudiness and Earth's energy balance, or how this link would change in a changing climate.

Conceptual models could be useful in elucidating how the main features of cloudiness connect to the energy balance, and how these connections may respond to large scale climatic changes. However, existing conceptual work on large-scale cloudiness is sparse. The majority of theory relevant to cloudiness is about the general circulation. Existing work has focused on specific regions or regimes, such as the tropics (Pierrehumbert, 1995; Miller, 1997), the Walker circulation (Peters & Bretherton, 2005), or the formation of midlatitude storms (Charney, 1947; Eady, 1949; Pierrehumbert & Swanson, 1995), among others, and further research may link circulation with cloud formation at large, but still local, scales (Carlson, 1980). What is missing is a conceptual framework that both closes the top-of-atmosphere energy budget (and hence by necessity considers the planet as a whole), but also includes clouds. A suitable candidate for such a framework would be a an energy balance model (Budyko, 1969; Sellers, 1969; Ghil, 1981; North & Kim, 2017) that explicitly represents dynamic cloudiness.

In this work we derive simple representations, or “recipes”, for global cloudiness, which can be potentially included in energy balance models, helping link variations in the energy budget and state variables of such models to variations in cloudiness and vice-versa. These representations therefore need to capture all main features of cloudiness, which are the global mean value, mean seasonal cycle, coarse spatial variability, and the difference between the shortwave and longwave impact of cloudiness. To derive them, we will use a quantitative top-down approach, where global cloudiness is directly decomposed into contributions from several simpler spatiotemporal fields. These fields are the “ingredients” of the recipe, which we refer to simply as predictors (in the sense of statistical predictors). A model useful in theoretical work is one that can explain the most with the least amount of information, and therefore in this work the main objective is to derive minimal representations that use a few predictors.

Similar top-down approaches have been used frequently in the literature in the context of the empirical cloud controlling factors framework (Stevens & Brenguier, 2009). For tropical low clouds there are several studies summarized in the review by Klein et al. (2017), and see also Myers et al. (2021) for ESMs vs. observations. Attention has also been given to the midlatitude cloudiness (a summary of existing work on extratropical cloud controlling factors can be found in Kelleher and Grise (2019) and see also Grise and Kelleher (2021) for ESMs vs. observations). Our approach differs from past empirical approaches in that we fit absolute cloudiness, not anomalies, and we fit cloudiness fields over all available space and time.

Section 2 describes how we define cloudiness, which predictors to consider, how to fit predictor models on observed cloudiness, and how to judge the quality of the fits. Then, Sect. 3 presents the main analysis and results on how well the models capture cloud albedo and cloud longwave radiative effect. A summary and discussion of potential impact for sensitivity studies concludes the paper in Sect. 4.

2 Fitting global cloudiness

2.1 Quantifying cloudiness

To fit any model, a definition of cloudiness that is both quantitatively precise but also energetically meaningful is required. For the shortwave part, we use the energetically consistent effective cloud albedo (in the following, just “cloud albedo”), C, estimated using the approach of Datseris and Stevens (2021). C is a better way to quantify shortwave impact of cloudiness than the shortwave cloud radiative effect (CRE), because a large amount of variability of the latter actually comes from the variability of insolation (Datseris & Stevens, 2021). For the longwave part the CRE, L, is a good representation of the radiative impact of clouds. From it, a cloud effective emissivity can be constructed which can be added to an energy balance model directly similarly to the albedo. Both C, L are derived from monthly-mean CERES EBAF data (Loeb et al., 2018) using 19 years of measurements (2001-2020).

2.2 Predictors considered

The predictors considered in this study, listed below, are obtained from ERA5 data (Hersbach et al., 2020) using 19 years of data (2001-2020). Pressure velocity ω_{500}, estimated inversion strength EIS, surface wind speed V_{sfc}, sea surface temperature SST, and stratospheric specific humidity q_{700}, have been used numerous times in the literature. ω_{500} is known to be important for both shortwave and longwave cloud radiative effects (Bony et al., 1997; Norris & Weaver, 2001; Bony et al., 2004; Norris & Iacobellis, 2005), and EIS, V_{sfc}, SST, q_{700} have been used to fit cloud cover anomalies in a variety of regimes, see e.g., Klein et al. (2017); Kelleher and Grise (2019) and references therein for a more detailed discussion. Do note that the connections between predictors and cloudiness in the literature are analyzed for specific regimes (such as tropical subsidence regions, or North midlatitudes, etc.), while here we depart from past work by testing their potential in fitting cloudiness globally.

We included CTE, the estimated cloud top entrainment index, because Kawai et al. (2017) present it as an improvement over EIS. Both $q_{700}, q_{\mathrm{tot}}$ (with q_{tot} the total column water vapor) are a proxy for the moisture of an atmospheric column, and expected to be relevant when fitting L. In our analysis however, q_{700} gives consistently better fits when used in place of q_{tot}, keeping all other aspects fixed (not shown). Thus, we will not discuss q_{tot} more in this study. Using specific humidity at 700hPa instead of at surface results in only minor improvement of fit quality throughout the analysis (also not shown).

The fraction of updrafts ω_{up} is useful because it is bounded in $[0\%, 100\%]$, like C, and given that we fit absolute values instead of anomalies, it does not penalize the fits with negative values (that exist in ω_{500}). It can also be used as a statistical weight to distinguish between regions of large scale subsidence, see e.g., Bony et al. (1997). The standard deviation of ω_{500}, ω_{std}, which can be thought of as a simple quantifier of storminess, has been shown to be a useful predictor of cloudiness by Norris and Iacobellis (2005) due to the nonlinear connection between vertical motion and cloud generation. Another argument favoring ω_{std} is that it relates cloudiness with the moisture of the air column better than ω_{500}, see Sect. 3.3.

2.3 Fitting process

Let Y be a measure of cloudiness (C of L from Sect. 2.1) and X_i be some predictor fields, for $i = 1, \ldots, n$,. Y, X_i are global spatiotemporal fields. We assume that with sufficient accuracy we can write

$$Y \approx M = f(X_1, \ldots, X_n; p_1, \ldots, p_m) \overset{\text{e.g.}}{=} p_1 X_1 + p_2 X_2 + p_3 X_1 X_2 \tag{1}$$

with p_j, for $j = 1, \ldots, m$ some parameters to be estimated (all $p_j \in \mathbb{R}$). In the following we call f the "cloud fitting function". Naturally, different forms for f and/or sets of predictors will yield a better fit for C or L respectively, as each captures different aspects of cloudiness. Given a specific form for f, and a set of predictors X_i, the parameters p_j of the model are estimated via a standardized nonlinear least square optimization (Levenberg, 1944; Marquardt, 1963). The minimization objective is the squared distance between Y derived from CERES observations, and M produced by Eq. 1. Details on the data pre-processing before doing the fits are provided in the Supplementary Information.

This approach of fitting models with free parameters to observed data is similar to the cloud controlling factors framework (CCFF), but there are some key differences with typical CCFF studies. First, we fit absolute cloudiness, not anomalies, and hence the mean value of Y, and its seasonal cycle, must be captured by the fit. The importance of capturing the mean value and mean seasonal cycle is further enforced by the fact that the inter-annual variability of cloudiness is small in decadal timescales (Stevens & Schwartz, 2012; Stephens et al., 2015), and hence the mean seasonal cycle captures the majority of the signal. Because we want to capture the mean, f is generally allowed to be nonlinear. Second, we fit across all available space and time without any restrictions to special regions of space or specific cloud types. We discuss in more detail the differences with typical CCFF studies in the Supplementary Information.

2.4 Quantitatively measuring fit quality

To quantify fit quality with an objective measure that is independent of what predictors are used, we chose the normalized root mean square error (NRMSE), defined as

$$\epsilon(Y, M) = \sqrt{\frac{\sum_n (Y_n - M_n)^2}{\sum_n (Y_n - \bar{Y})^2}} \tag{2}$$

with Y, M as in Eq. 1, $\bar{Y}$ the mean of Y and n enumerates the data points. This error measure is used routinely in e.g., spatiotemporal timeseries prediction (Isensee et al., 2019), and is a statistic agnostic of the values of Y, M that can compare fit quality across different ways of fitting. If $\epsilon > 1$ the mean value of Y is a better model than M (equivalently, the variance of the observations is smaller than the mean square error between fit and observations). There are several ways to compute ϵ: on full spatiotemporal data, on zonally and temporally averaged data, or on the seasonal cycles of tropics (0^o-30^o) and midlatitudes (30^o-70^o). Each measure highlights a different aspect of fit quality and all measures were taken into account when deciding the best fits.

3 Results & Discussion

In this section we present the "best" fits for cloud albedo C and longwave cloud radiative effect L. The "best" fits are the most minimal fits, that accommodate intuitive physical justification, but also provide good fit quality (i.e., low values for ϵ). Only the requirement is small error ϵ is objective, while the rest have at least partly a subjective nature. Additionally, fits that use simpler predictors, that can be more straightforwardly represented in a conceptual framework, are preferred. If two fits have approximately equal error ϵ, but one uses a simpler predictor (e.g., surface temperature SST versus atmospheric specific humidity q_{700}), the first fit is "better".

3.1 Two predictor linear model

The simplest model one can use for the cloud fitting function f is one that combines two predictors and two free parameters in a linear manner: $f = p_1 X_1 + p_2 X_2$. Even if this model does not yield a good fit for cloudiness, it is advantageous to start with it nevertheless. All possible linear combinations given all possible predictors of Sect. 2.2 are only 36, and they can already highlight which predictors are worth a closer look for which measure of cloudiness. The results are in Fig. 1, which showcases two different error measures (error in temporally and zonally mean cloudiness, and median of errors in seasonal cycle of cloudiness), and how these errors depend on which predictors are used for the linear fit.

The majority of combinations result in low fit quality ($\epsilon \geq 0.9$). Nevertheless, Fig. 1 reveals some useful information. For C, a measure of the inversion strength is necessary for a decent fit and the combination of ω_{up} and CTE result in the best case scenario. For L, the most important predictor seems to be ω_{std}, which gives decent fits in both space and time for a wide selection of second predictors (while ω_{500} gives decent fits only in time). A second important predictor for L seems to be q_{700} or SST.

3.2 Best fit for cloud albedo C

While it is already clear in the literature that ω_{500} is an important predictor for shortwave impact of clouds (Sect. 2.2), the fact that ω_{up} performs so much better in a linear model hints that the bounded nature of albedo, $C \in [0\%, 100\%]$, is important. Negative predictor values yield low fit quality and also penalize fitting well positive values. One way to counter this would be to use ω_{up} as probability weight multiplying other predictors. An alternative would be to use appropriate nonlinear functions of the more

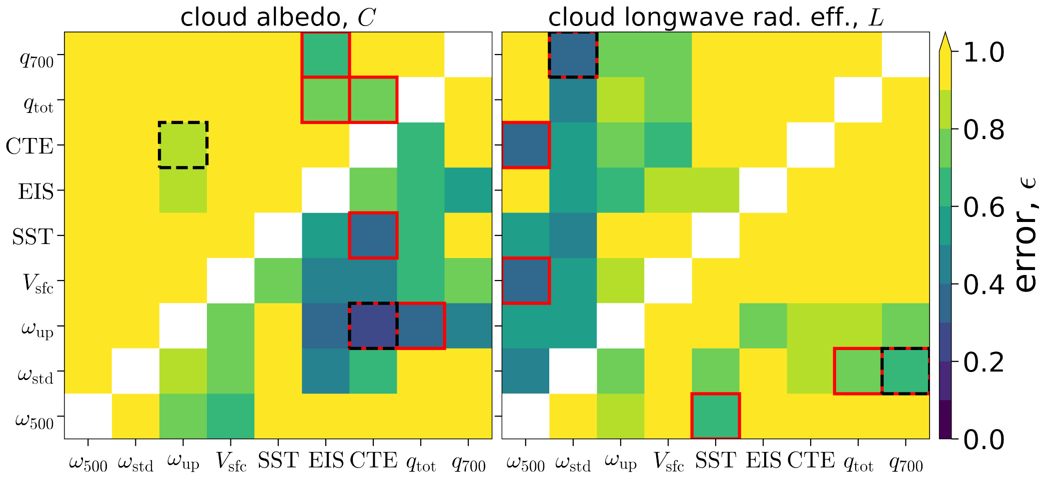

Figure 1. Error in temporally and zonally mean cloudiness (lower-right triangle of heatmap), and error in mean seasonal cycle (upper-left triangle of heatmap), as a function of which predictors of the x and y axis combine into a linear model $f = p_1 X_1 + p_2 X_2$ for fitting cloud albedo (left plot) or longwave cloud radiative effect (right plot). Red outline highlights the three combinations with the lowest error in each category, while black dashed outline highlights the combination with lowest error overall (by multiplying the two errors). It is possible that $e > 1$ because we are fitting without intercept.

basic ω_{500}. Regardless the choice, CTE must also be included in the model, as it is necessary to capture the important contribution of low clouds.

A model that satisfies all these requirements, and achieves the best fit, is

$$C = 50p_1\left(\tanh(p_2\omega_{500} + p_3\mathrm{CTE}) + 1\right) \tag{3}$$

where we used the nonlinear function $x \to 50(\tanh(x)+1)$ to map predictors to $[0\%, 100\%]$. The results of the fit (i.e., estimating the parameters p_1, p_2, p_3 that give least square error between Eq. 3 and the observed CERES C) are in Fig. 2. The model fit captures all main features of cloud albedo, and achieves $\epsilon = 0.54$ over the full space and time, $\epsilon = 0.19$ in the zonal and temporal average, and $\epsilon = 0.65$ in seasonal cycle. The shortwave cloud radiative effect (which in our study is simply the multiplication of C with the insolation I, and then averaging), is 57.1 W/m^2 in CERES and 57.45 W/m^2 when using the model fit. The inclusion of the parameter p_1 is necessary, because in observations cloud albedo does not saturate to 100%, but to much lower values (see Fig. 2). We also note that using EIS instead of CTE in the model decreases fit quality significantly, because, while EIS and CTE both capture subtropical low cloud albedo well, only CTE also captures midlatitude low cloud albedo well, while EIS does not. Thus, as suggested by Kawai et al. (2017), CTE is indeed an improvement over EIS.

Adding more predictors increases fit quality only slightly. E.g., adding a factor $p_4 V_{\mathrm{sfc}}$ inside the tanh function decreases time and zonal mean error to $\epsilon = 0.18$ from $\epsilon = 0.19$ and seasonal cycle error to $e = 0.6$ from $e = 0.65$, as well as captures hemispheric asymmetries in C slightly better. That the decrease in error is so small gives confidence that that the basic physics governing cloud albedo are already captured by Eq. 3. Further fine-tuning of the model only captures higher order details that will likely not be included in a conceptual theory anyway.

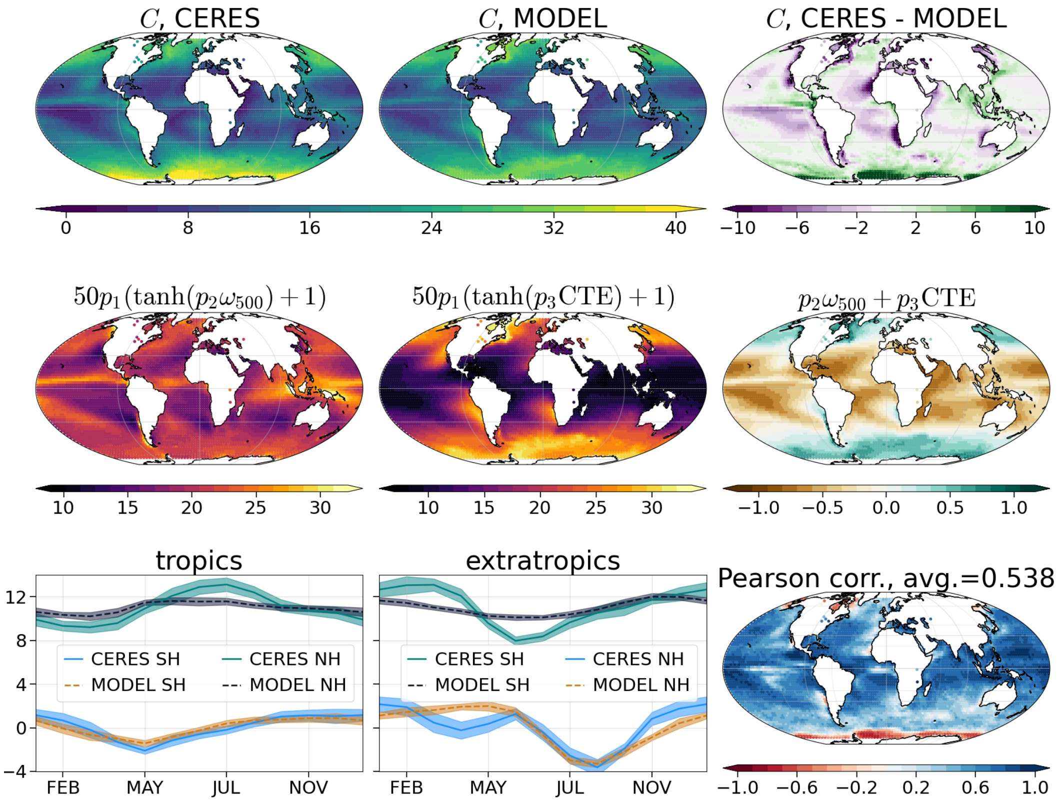

Figure 2. Results of fitting cloud albedo C (units of %) with the simple model of Eq. 3. First row are time-averaged maps. See also Fig. 4 for a zonally averaged version. Second row are the contributions of different terms in the model. Third row shows how well the model captures temporal variability. First two panels are the mean seasonal cycles (with semi-transparent bands noting the standard deviation around each month) in the tropics (0-30°) and extratropics (30-70°). The mean value of all cycles has been subtracted, and SH cycles are offset for visual clarity. The third panel is a map of the Pearson linear correlation coefficient between the time-series of the model and CERES data at each grid point. Units of ω_{500} in Pa/s and CTE in K, and $p_1 = 0.4, p_2 = 6.87, p_3 = 0.08$. We multiply ω_{500} with -1 before any analysis so that $\omega_{500} > 0$ means updrafts.

The middle row of Fig. 2 provides some insights on the contribution of each predictor. Both CTE and ω_{500} contribute to midlatitude cloud albedo, but CTE slightly more so. In the tropics ω_{500} contributes the albedo of the convective regimes (ITCZ, Maritime Continent), and CTE the albedo of the low stratocumulus decks (subsidence regions). CTE is in some sense a more important predictor than ω_{500}, because if we set explicitly $p_2 = 0$ in Eq. 3, we get lower error of $\epsilon = 0.7$ in full space and time, versus the error of $\epsilon = 0.9$ we would get if we set explicitly $p_3 = 0$ instead. Alternative models to Eq. 3 can give similar results using ω_{up} instead of ω_{500}. For example, using $f = p_1\omega_{\mathrm{up}} + p_2\mathrm{CTE}(1-\omega_{\mathrm{up}})$ provides similar, but slightly worse, fit quality with $\epsilon = 0.57$ over full space and time and $\epsilon = 0.23$ over time and zonal mean. However, ω_{500} is a simpler predictor than ω_{up}, and hence a model with ω_{500} is more minimal (and thus, "better").

3.3 Best fit for longwave cloud radiative effect L

Fitting L is more complex for mainly two reasons. First, the longwave effect of a cloud depends strongly on the infrared opacity, and hence moisture content, of the atmospheric column overshadowed by the cloud. Moisture content though is, at least partly, controlled by temperature. Warm and humid atmospheres are already almost opaque to longwave radiation, and hence the presence of a cloud would make little difference. In contrast, in a cold and dry atmosphere a cloud would bring a lot of extra absorption of outgoing longwave radiation and hence large L. Second, cloud height matters a lot for its effective emissivity (as cloud height sets its temperature), while cloud height does not have a significant effect on cloud albedo (keeping all other factors fixed).

These considerations likely explain why we were not able to find a model that had as good of a fit for L as it had for C when restricting the model to using at most two predictors. After an analysis of several different linear and nonlinear combinations, the "best" model we could construct was of the form

$$L = p_1\omega_{\mathrm{std}} + p_2\omega_{500} + p_3\mathrm{SST} \tag{4}$$

(notice how Eq. 4 has 0 intercept by force, so that it must capture the mean from the predictors, and not from a tunable parameter). The results of the fit are in Fig. 3. Similarly with C, the fit captures all main features of L. The fit errors are $e = 0.63$ over full space and time, $e = 0.46$ in time and zonal mean and $e = 0.41$ in mean seasonal cycle. The mean LCRE is 27.27 W/m^2 in CERES and 27.30 in our model fit W/m^2. Spatial variability is captured worse for L versus C, but temporal variability is captured better. A factor that contributes to this is that the temporal variability of L is much simpler than it is for C (e.g., relative power of 12-month periodic component is much larger in L timeseries, leading to simpler seasonal cycle temporal structure).

We now give some physical intuition on the choice of predictors. Monthly-mean ω_{500} is a proxy to cloud height (persistent updrafts and with larger magnitude should result in higher clouds). The surface temperature SST is a proxy for the emissivity of the air column without a cloud, because the potential total moisture content of atmospheric columns is a monotonically increasing function of temperature under first approximation. Using q_{700} instead of SST captures spatial variability worse but improves the capturing of temporal variability. Given that SST is a more basic predictor than q_{700}, and is directly represented in conceptual energy balance models, SST is preferred. Furthermore, and as was the case with C, adding more predictors, or additional nonlinear terms of existing predictors such as a factor $p_4\omega_{\mathrm{std}}\mathrm{SST}$, increases fit quality but only slightly.

Interestingly, ω_{std} is the most important predictor for L. Even though ω_{500} captures a broader range of values (~ 40 versus the ~ 30 of ω_{std}), absence of ω_{std} significantly lowers fit quality in all combinations of cloud fitting functions f and predictors we tested, even when including ω_{500} in all of them. The spatial structure of ω_{std} is the most similar to the spatial structure of L, with the main difference being that for ω_{std} the peak values in tropics and extratropics have equal magnitude, while for L the tropics peak values have 33% more magnitude. Hence, some other predictor must lower the extratropical magnitude of ω_{std}, and here this role is fullfilled by SST in Eq. 4 (or q_{700}, if one uses it instead of SST).

A physical connection between ω_{std} and L can be thought of as follows: persistent updrafts, that are captured by ω_{500}, lead to a moist atmosphere and hence weak L, mostly irrespectively of cloud height. On the other hand, consistent pumping of air up and down (high ω_{std}, but almost zero ω_{500}) would leave the atmosphere dry (for at least half the time), but the formed clouds would linger longer above the dry atmosphere and have a disproportionately strong effect, yielding high L. In the midlatitudes both L and ω_{std} have their latitudinal maximum in the middle of the Ferrel cell (40-45°), where $\omega_{500} \approx 0$. Of course, monthly-mean $\omega_{500} \approx 0$, but in the hourly timescale there is a lot of ver-

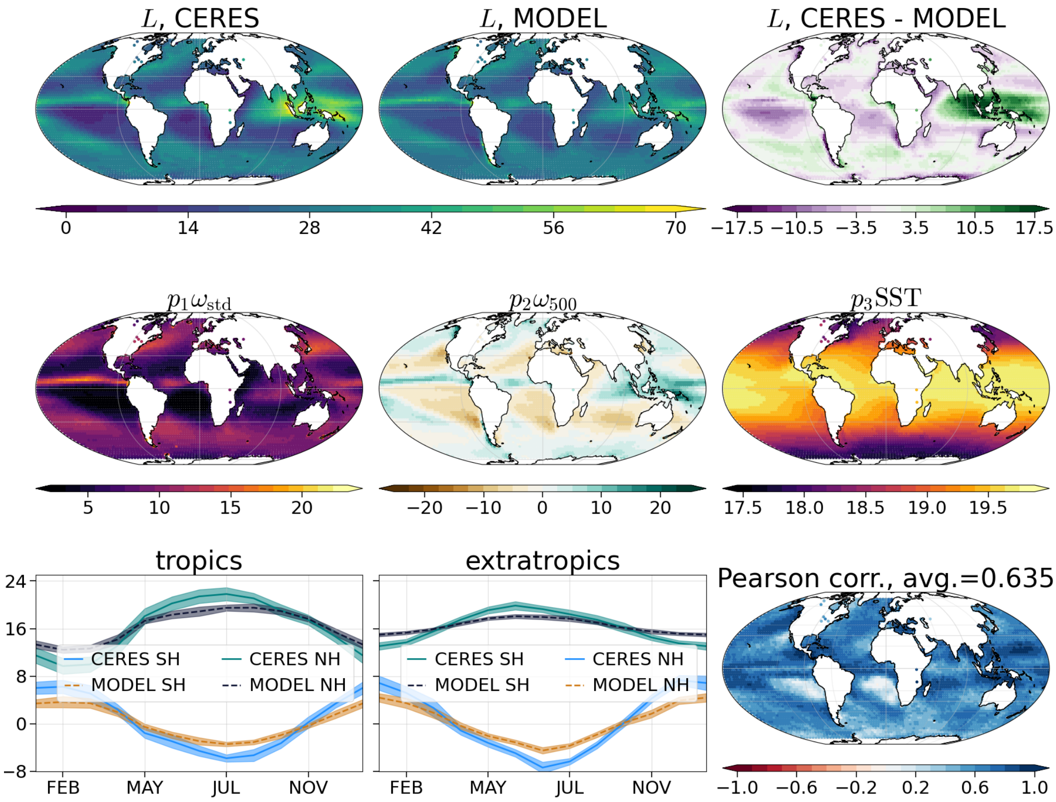

Figure 3. As in Figure 2 but now for longwave cloud radiative effect L. Units of L in W/m^2, $\omega_{500}, \omega_{\mathrm{std}}$ in Pa/s, SST in K, and $p_1 = 42.68, p_2 = 208.9, p_3 = 0.06558$.

tical motion, as captured by the high values of ω_{std}. This reflects the fact that the center of the Ferrell cell coincides with the centre of the midlatitude storm tracks. In the tropics, ω_{500} and ω_{std} have little differences in their latitudinal structure.

3.4 Comparison with ERA5 and reduced data

For obtaining reference values of the errors we report here, we also compare the outcome of our analysis with using direct ERA5 radiation output to measure C or L. Calculating L is straightforward, however, we cannot compute the energetically consistent effective cloud albedo from ERA5, because it requires cloud optical depth, a field not exported by ERA5. Instead, we can compute the cloud contribution to atmospheric albedo α^{CLD} (specifically, Eq. 3 from Datseris and Stevens (2021)), which has only small differences with C. α^{CLD} also has the downside of not having a time dimension due to absence of sunlight for large portions of the data(Datseris & Stevens, 2021).

We also present fits and their errors for fitting reduced data directly, specifically temporally and zonally averaged data. Fitting reduced data increases fit quality, because this case neglects higher-order effects that contribute to e.g. zonal or temporal structure. If, however, the fit quality increases only slightly, that gives confidence that the basic connections captured by our models are indeed the most important ones and hence also dominate full spatiotemporal variability. The results are in Fig. 4.

Two conclusions can be readily drawn: (1) our fits have smaller error ϵ than does the cloudiness inferred from ERA5 radiation output, (2) fitting the simplified version of

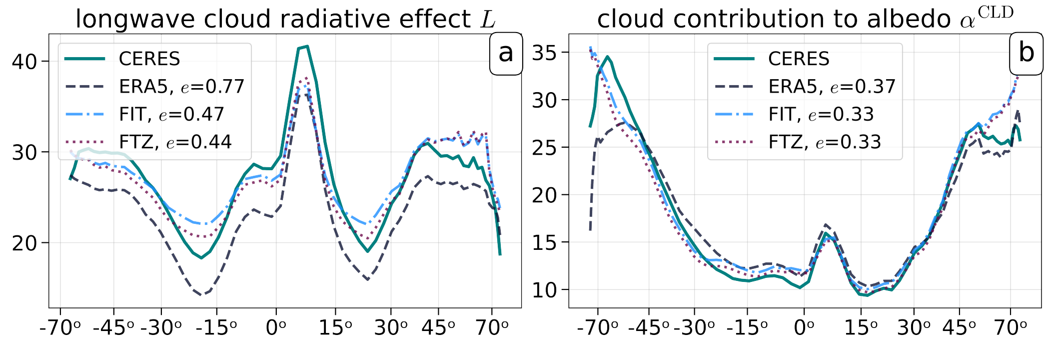

Figure 4. Temporally and zonally averaged data (and their errors e, Eq. 2, versus the CERES curve) of CERES, our model fits, and direct ERA5 output for (a) the longwave cloud radiative effect L and (b) the cloud contribution to atmospheric albedo α^{CLD}. In (a), "FIT" is over all space and time, and "FTZ" is a fit over temporally and zonally averaged data. In (b), "FIT" is a fit over temporally averaged data (no time information can be used), and "FTZ" is as before.

temporally and zonally averaged data increases fit quality only slightly, further validating the fit quality. Additionally, the best parameters of the fits change little when doing the zonal-only fit (e.g., for C, parameters become $p_1 = 0.4, p_2 = 8.25, p_3 = 0.077$ versus those reported in Fig. 2). This means that the contribution of each predictor does not change fundamentally in the reduced version, giving us even more confidence that the simple models of Eqs. 3, 4 capture the basic physics well.

4 Conclusions

The goal of this work was to identify ways one can accurately represent observed global cloudiness using as few and as simple components as possible. We have shown that the combination of pressure velocity ω_{500} and a measure of temperature inversion CTE are enough to capture all main features of cloud albedo, while surface temperature SST, standard deviation of hourly pressure velocity ω_{std}, and ω_{500}, capture all main features of longwave cloud radiative effect. Our model fits naturally have some discrepancies with observations, but none are major. E.g., southern ocean C is underestimated, temporal variability of C is not captured well, especially in southern ocean, L of Maritime Continent is underestimated, among others. Even though we only fitted over ocean here, in fact the fits do not perform much worse when considering the whole planet without adding more information to the cloud fitting functions f (not shown). We also note that the predictors used in the presented models were favored because of their simplicity, but also because they can be potentially connected with equator-to-pole temperature gradients. This may allow incorporating cloudiness in energy balance models, a possibility which we outline in the Supplementary Information.

Equations 3 and 4, and the analysis of Sect. 3, can also be used to quantify the response of cloudiness to a change in the climate system. For example, quantify how a change in the variability of the circulation or inversion strength would impact global cloudiness and hence the energy balance. But also, the equations can provide spatially localized information on such changes, such as in which areas of the globe would circulation changes impact global cloudiness the most. These applications seem useful for e.g., better quantifying cloud sensitivities in the context of global warming.

The exact parameter values p_j in Eqs. 3 and 4 have been derived from fitting on current climate and their values may change for different climates. Thankfully, this change is not very large. We confirmed that by doing the fit of Sect. 3.2, but for each hemisphere individually. As far as circulation patterns and cloudiness distributions are concerned, the two hemispheres have significant differences. Recall that the parameters of the fit for the whole globe were $p = \{0.4, 6.87, 0.08\}$. For only north hemisphere, we obtained $\{0.38, 7, 0.07\}$ and for only south $\{0.41, 6.89, 0.086\}$. Because the parameter sets have little differences in each case, this gives more confidence that the equations capture the basic physical connections instead of being a case of overfitting.

Acknowledgments

We thank Hauke Schmidt for helpful discussions. The datasets used were monthly mean CERES EBAF (Loeb et al., 2018; Kato et al., 2018; Doelling et al., 2013; Rutan et al., 2015) for surface & top of the atmosphere radiation fields, and cloud properties, monthly mean ERA5 (Hersbach et al., 2020) for temperature, pressure, humidity, and hourly mean ERA5 for pressure velocity. The code we used is available online (Datseris, 2022). It uses the Julia language (Bezanson et al., 2017), and the packages: GLM.jl, LsqFit.jl, ClimateBase.jl, and DrWatson (Datseris et al., 2020). Figures were produced with the matplotlib library (Hunter, 2007). The code can also be be used to fit any arbitrary spatiotemporal field with any combination of functional forms and predictor fields.

Author contributions. G.D. performed the primary analysis and wrote the first draft. All authors contributed key ideas that shaped the study, and helped revise the draft.

References

Bezanson, J., Edelman, A., Karpinski, S., & Shah, V. B. (2017). Julia: A fresh approach to numerical computing. *SIAM Review*, *59*(1), 65–98. Retrieved from `https://epubs.siam.org/doi/10.1137/141000671` doi: 10.1137/141000671

Bony, S., Dufresne, J.-L., Treut, H. L., Morcrette, J.-J., & Senior, C. (2004, March). On dynamic and thermodynamic components of cloud changes. *Climate Dynamics*, *22*(2-3), 71–86. Retrieved from `https://doi.org/10.1007/s00382-003-0369-6` doi: 10.1007/s00382-003-0369-6

Bony, S., Lau, K.-M., & Sud, Y. C. (1997). Sea surface temperature and large-scale circulation influences on tropical greenhouse effect and cloud radiative forcing. *Journal of Climate*, *10*(8), 2055 - 2077. Retrieved from `https://journals.ametsoc.org/view/journals/clim/10/8/1520-0442_1997_010_2055_sstals_2.0.co_2.xml` doi: 10.1175/1520-0442(1997)010⟨2055:SSTALS⟩2.0.CO;2

Budyko, M. I. (1969). The effect of solar radiation variations on the climate of the Earth. *Tellus*, *21*(5), 611–619. doi: 10.3402/tellusa.v21i5.10109

Carlson, T. N. (1980). Airflow through midlatitude cyclones and the comma cloud pattern. *Monthly Weather Review*, *108*(10), 1498 - 1509. Retrieved from `https://journals.ametsoc.org/view/journals/mwre/108/10/1520-0493_1980_108_1498_atmcat_2_0_co_2.xml` doi: 10.1175/1520-0493(1980)108⟨1498:ATMCAT⟩2.0.CO;2

Charney, J. G. (1947, oct). The dynamics of long waves in a baroclinic westerly current. *Journal of the Atmospheric Sciences*, *4*(5), 136–162. Retrieved from `http://journals.ametsoc.org/doi/10.1175/1520-0469(1947)004%3C0136:TDOLWI%3E2.0.CO;2` doi: 10.1175/1520-0469(1947)004⟨0136:TDOLWI⟩2.0.CO;2

Cotton, W. R., Bryan, G., & Van Den Heever, S. C. (2014). *Storm and cloud dynamics* (2nd ed.). Academic Press.

Datseris, G. (2022). *Code for our paper "minimal recipes for global cloudiness"*. Zenodo. doi: 10.5281/zenodo.6565962

Datseris, G., Isensee, J., Pech, S., & Gál, T. (2020). Drwatson: the perfect sidekick for your scientific inquiries. *Journal of Open Source Software*, *5*(54), 2673. Retrieved from `https://doi.org/10.21105/joss.02673` doi: 10.21105/joss.02673

Datseris, G., & Stevens, B. (2021, August). Earth's albedo and its symmetry. *AGU Advances*, *2*(3). Retrieved from `https://doi.org/10.1029/2021av000440` doi: 10.1029/2021av000440

Doelling, D. R., Loeb, N. G., Keyes, D. F., Nordeen, M. L., Morstad, D., Nguyen, C., ... Sun, M. (2013, June). Geostationary enhanced temporal interpolation for CERES flux products. *Journal of Atmospheric and Oceanic Technology*, *30*(6), 1072–1090. Retrieved from `https://doi.org/10.1175/jtech-d-12-00136.1` doi: 10.1175/jtech-d-12-00136.1

Eady, E. T. (1949). Long waves and cyclone waves. *Tellus*, *1*(3), 33–52.

Ghil, M. (1981). Energy-Balance Models: An Introduction. In *Climatic variations and variability: Facts and theories* (pp. 461–480). Dordrecht: Springer Netherlands. Retrieved from `http://link.springer.com/10.1007/978-94-009-8514-8_27` doi: 10.1007/978-94-009-8514-8_27

Grise, K. M., & Kelleher, M. K. (2021). Midlatitude cloud radiative effect sensitivity to cloud controlling factors in observations and models: Relationship with southern hemisphere jet shifts and climate sensitivity. *Journal of Climate*, *34*(14), 5869–5886. doi: 10.1175/JCLI-D-20-0986.1

Hersbach, H., Bell, B., Berrisford, P., Hirahara, S., Horányi, A., Muñoz-Sabater, J., ... Thépaut, J.-N. (2020, June). The ERA5 global reanalysis. *Quarterly Journal of the Royal Meteorological Society*, *146*(730), 1999–2049. Retrieved from `https://doi.org/10.1002/qj.3803` doi: 10.1002/qj.3803

Houze, R. A., Jr. (2014). *Cloud dynamics* (2nd ed.). Academic Press.

Hunter, J. D. (2007). Matplotlib: A 2d graphics environment. *Computing in Science & Engineering*, *9*(3), 90–95. doi: 10.1109/MCSE.2007.55

Isensee, J., Datseris, G., & Parlitz, U. (2019, October). Predicting spatio-temporal time series using dimension reduced local states. *Journal of Nonlinear Science*, *30*(3), 713–735. Retrieved from `https://doi.org/10.1007/s00332-019-09588-7` doi: 10.1007/s00332-019-09588-7

Kato, S., Rose, F. G., Rutan, D. A., Thorsen, T. J., Loeb, N. G., Doelling, D. R., ... Ham, S.-H. (2018, May). Surface irradiances of edition 4.0 clouds and the earth's radiant energy system (CERES) energy balanced and filled (EBAF) data product. *Journal of Climate*, *31*(11), 4501–4527. Retrieved from `https://doi.org/10.1175/jcli-d-17-0523.1` doi: 10.1175/jcli-d-17-0523.1

Kawai, H., Koshiro, T., & Webb, M. J. (2017, November). Interpretation of factors controlling low cloud cover and low cloud feedback using a unified predictive index. *Journal of Climate*, *30*(22), 9119–9131. Retrieved from `https://doi.org/10.1175/jcli-d-16-0825.1` doi: 10.1175/jcli-d-16-0825.1

Kelleher, M. K., & Grise, K. M. (2019). Examining Southern Ocean cloud controlling factors on daily time scales and their connections to midlatitude weather systems. *Journal of Climate*, *32*(16), 5145–5160. doi: 10.1175/JCLI-D-18-0840.1

Klein, S. A., Hall, A., Norris, J. R., & Pincus, R. (2017). Low-Cloud Feedbacks from Cloud-Controlling Factors: A Review. *Surveys in Geophysics*, *38*(6), 1307–1329. doi: 10.1007/s10712-017-9433-3

Levenberg, K. (1944). A method for the solution of certain non-linear problems in least squares. *Quarterly of Applied Mathematics*, *2*(2), 164–168. Retrieved from `https://doi.org/10.1090/qam/10666` doi: 10.1090/qam/10666

Loeb, N. G., Doelling, D. R., Wang, H., Su, W., Nguyen, C., Corbett, J. G., ... Kato, S. (2018, January). Clouds and the earth's radiant energy system (CERES) energy balanced and filled (EBAF) top-of-atmosphere (TOA) edition-4.0 data product. *Journal of Climate*, *31*(2), 895–918. Retrieved from https://doi.org/10.1175/jcli-d-17-0208.1 doi: 10.1175/jcli-d-17-0208.1

Marquardt, D. W. (1963, June). An algorithm for least-squares estimation of nonlinear parameters. *Journal of the Society for Industrial and Applied Mathematics*, *11*(2), 431–441. Retrieved from https://doi.org/10.1137/0111030 doi: 10.1137/0111030

Miller, R. L. (1997). Tropical thermostats and low cloud cover. *Journal of Climate*, *10*(3), 409–440. doi: 10.1175/1520-0442(1997)010⟨0409:TTALCC⟩2.0.CO;2

Myers, T. A., Scott, R. C., Zelinka, M. D., Klein, S. A., Norris, J. R., & Caldwell, P. M. (2021). Observational constraints on low cloud feedback reduce uncertainty of climate sensitivity. *Nature Climate Change*, *11*(6), 501–507. Retrieved from http://dx.doi.org/10.1038/s41558-021-01039-0 doi: 10.1038/s41558-021-01039-0

Norris, J. R., & Iacobellis, S. F. (2005, November). North pacific cloud feedbacks inferred from synoptic-scale dynamic and thermodynamic relationships. *Journal of Climate*, *18*(22), 4862–4878. Retrieved from https://doi.org/10.1175/jcli3558.1 doi: 10.1175/jcli3558.1

Norris, J. R., & Weaver, C. P. (2001). Improved techniques for evaluating GCM cloudiness applied to the NCAR CCM3. *Journal of Climate*, *14*(12), 2540–2550. doi: 10.1175/1520-0442(2001)014⟨2540:ITFEGC⟩2.0.CO;2

North, G., & Kim, K.-Y. (2017). *Energy balance climate models*. Weinheim, Germany: Wiley-VCH.

Peters, M. E., & Bretherton, C. S. (2005). A simplified model of the Walker circulation with an interactive ocean mixed layer and cloud-radiative feedbacks. *Journal of Climate*, *18*(20), 4216–4234. doi: 10.1175/JCLI3534.1

Pierrehumbert. (1995, may). Thermostats, Radiator Fins, and the Local Runaway Greenhouse. *Journal of the Atmospheric Sciences*, *52*(10), 1784–1806. Retrieved from http://journals.ametsoc.org/doi/10.1175/1520-0469(1995)052%3C1784:TRFATL%3E2.0.CO;2 doi: 10.1175/1520-0469(1995)052⟨1784:TRFATL⟩2.0.CO;2

Pierrehumbert, & Swanson. (1995, jan). Baroclinic Instability. *Annual Review of Fluid Mechanics*, *27*(1), 419–467. Retrieved from http://fluid.annualreviews.org/cgi/doi/10.1146/annurev.fluid.27.1.419 doi: 10.1146/annurev.fluid.27.1.419

Rutan, D. A., Kato, S., Doelling, D. R., Rose, F. G., Nguyen, L. T., Caldwell, T. E., & Loeb, N. G. (2015, June). CERES synoptic product: Methodology and validation of surface radiant flux. *Journal of Atmospheric and Oceanic Technology*, *32*(6), 1121–1143. Retrieved from https://doi.org/10.1175/jtech-d-14-00165.1 doi: 10.1175/jtech-d-14-00165.1

Sellers, W. D. (1969, jun). A Global Climatic Model Based on the Energy Balance of the Earth-Atmosphere System. *Journal of Applied Meteorology*, *8*(3), 392–400. Retrieved from http://journals.ametsoc.org/doi/abs/10.1175/1520-0450{\%}281969{\%}29008{\%}3C0392{\%}3AAGCMBO{\%}3E2.0.CO{\%}3B2http://journals.ametsoc.org/doi/10.1175/1520-0450(1969)008{\%}3C0392:AGCMBO{\%}3E2.0.CO;2 doi: 10.1175/1520-0450(1969)008⟨0392:AGCMBO⟩2.0.CO;2

Sherwood, S. C., Webb, M. J., Annan, J. D., Armour, K. C., Forster, P. M., Hargreaves, J. C., … Zelinka, M. D. (2020, December). An assessment of earth's climate sensitivity using multiple lines of evidence. *Rev. Geophys.*, *58*(4).

Siebesma, A. P., Bony, S., Jakob, C., & Stevens, B. (Eds.). (2020). *Clouds and climate*. Cambridge University Press. Retrieved from https://doi.org/10.1017/9781107447738 doi: 10.1017/9781107447738

Stephens, G. L., O'Brien, D., Webster, P. J., Pilewski, P., Kato, S., & Li, J.-l. (2015, mar). The albedo of Earth. *Reviews of Geophysics*, *53*(1), 141–163. Retrieved from http://doi.wiley.com/10.1002/2014RG000449 doi: 10.1002/2014RG000449

Stevens, B., & Brenguier, J.-L. (2009). Cloud-controlling factors: low clouds. In J. Heintzenberg & R. J. Charlson (Eds.), *Clouds in the perturbed climate system* (chap. 8). The MIT Press. Retrieved from `https://doi.org/10.7551/mitpress/9780262012874.001.0001` doi: 10.7551/mitpress/9780262012874.001.0001

Stevens, B., & Schwartz, S. E. (2012, May). Observing and modeling earth's energy flows. *Surveys in Geophysics*, *33*(3-4), 779–816. Retrieved from `https://doi.org/10.1007/s10712-012-9184-0` doi: 10.1007/s10712-012-9184-0

Zelinka, M. D., Myers, T. A., McCoy, D. T., Po-Chedley, S., Caldwell, P. M., Ceppi, P., … Taylor, K. E. (2020, January). Causes of higher climate sensitivity in CMIP6 models. *Geophys. Res. Lett.*, *47*(1).

Supplementary Information: Minimal recipes for global cloudiness

George Datseris[1], Joaquin Blanco[2], Or Hadas[3], Sadrine Bony[4], Rodrigo Caballero[2], Yohai Kaspi[3], Bjorn Stevens[4]

[1]Max Planck Institute for Meteorology, Hamburg, Germany
[2]Department of Meteorology, Stockholm University, Stockholm, Sweden
[3]Department of Earth and Planetary Sciences, Weizmann Institute of Science, Rehovot, Israel
[4]Sorbonne University, LMD/IPSL, CNRS, Paris, France

1 Table of fields

For convenience, in Table 1 we list all fields used in our study.

Symbol	Description	Reference
C	Energetically consistent effective cloud albedo	Datseris and Stevens (2021)
L	Longwave cloud radiative effect	Loeb et al. (2018)
ω_{500}	Pressure velocity at 500hPa	Grise and Kelleher (2021)
ω_{std}	Standard deviation of ω_{500} within a month	Norris and Iacobellis (2005)
ω_{up}	Fraction of updrafts of ω_{500} within a month	Bony et al. (1997)
V_{sfc}	10-meter wind speed	Brueck et al. (2015)
SST	Sea surface temperature (SST)	Qu et al. (2015)
q_{tot}	Total column water vapor	-
q_{700}	Specific humidity at 700hPa	Myers and Norris (2016)
EIS	Estimated inversion strength	Wood and Bretherton (2006)
CTE	Estimated cloud top entrainment index	Kawai et al. (2017)

Table 1. Fields to-be-predicted (C, L) and predictors considered in this study. An indicative reference for each is given as well. We multiply ω_{500} with -1 in this study, so that $\omega_{500} > 0$ means upwards motion.

2 Data pre-processing

All predictors, with the exception of ω_{std}, ω_{up}, are obtained from monthly-mean ERA5 data. The standard deviation ω_{std}, and fraction of updrafts ω_{up}, of ω_{500}, are derived from hourly ω_{500} data, aggregated over monthly periods. Using up to 6-hourly sampled data yields little quantitative difference in $\omega_{\text{std}}, \omega_{\text{up}}$.

All data, including the CERES EBAF monthly-mean data, have been transformed into an equal area grid of cell size $\approx$ 250km, from their standard orthogonal longitude-latitude grids. This is very important, otherwise statistical weights need to be used in the nonlinear least squares optimization process. Additionally, only data over ocean (a spatiotemporal mask is defined when CERES auxiliary ocean fraction is $> 50\%$) are considered, as, favoring simplicity, we would like to derive minimal models that do not deal with the complexities of including a land type contribution. Data were also limited to $\pm$ 70$^{\text{o}}$, to avoid potential CERES measurement artifacts near the poles.

Corresponding author: George Datseris, george.datseris@mpimet.mpg.de

3 Comparison with Cloud Controlling Factors Framework

At a fundamental level, our methodological approach (described in Sect. 2.3 of main text) is similar with the well-known Cloud Controlling Factors Framework (CCFF) (Stevens & Brenguier, 2009; Klein et al., 2017). We are fitting some measure of cloudiness using a function of predictors. However, there are some key differences worth highlighting in more detail.

The first is that the data used here are not anomalies. This means that the mean value of Y, and its seasonal cycle, must be captured by the fit. The importance of capturing the mean value and mean seasonal cycle is further enforced by the fact that the inter-annual variability of cloudiness is small in decadal timescales (Stevens & Schwartz, 2012; Stephens et al., 2015), and hence the mean seasonal cycle captures the majority of the signal (e.g., for hemispherically averaged all-sky reflected shortwave radiation, 99% of the variability (Datseris & Stevens, 2021)). Since the cloud fitting function is expected to capture the mean, it can be a nonlinear function (and if it is linear, then it must have intercept 0 by force). Another argument behind allowing nonlinear functions is that, generally speaking, a theory of cloudiness should be able to predict cloudiness over a broad range of different climatic states, not just small deviations from a reference climate (which justifies using a linear framework).

A second difference with typical CCFF studies is that we fit across all available space and time without any restrictions to special regions of space or cloud types (i.e., f does not depend on space). Typically in CCFF the fitted parameters (which are linear coefficients) are either aggregated over some specific region of Earth (e.g., subtropical subsidence regions like in Myers and Norris (2016)), or are fitted for each spatial point of the planet (e.g., like in Grise and Kelleher (2021)), or the focus is exclusively on a specific cloud type (e.g., low clouds like in Myers et al. (2021)). A third difference is that the cloud fraction (or cloud cover) is never considered as a quantifier of cloudiness, while the majority of CCFF studies use cloud fraction as the predictive field. Cloud fraction however does not have any energetic meaning, and cannot be used to connect clouds to the energy balance, and as a consequence, also cannot be used in a conceptual energy balance model.

4 Potential connection with energy balance models

In the introduction of the main text we discussed the benefits of including cloudiness in an energy balance model. There are two steps in achieving this in practice. First, express cloudiness as a function of simpler physical quantities. Second, represent these quantities in an energy balance model. In this work we achieved the first step. To accomplish the second step, one would have to express predictors $\omega_{500}, \omega_{\mathrm{std}}, \mathrm{CTE}$ as functions of temperature, or temperature differences (which are the typical state variables of energy balance models). While this task is certainly a subject of future research on its own right, the choice of predictors was such that there are physically sensible qualitative connections to start from. The discussion of this section may help guide future work on the subject.

The theory behind the baroclinic instability (Charney, 1947; Eady, 1949; Pierrehumbert & Swanson, 1995) states that midlatitude storms are driven by the equator-to-pole temperature gradient. Hence, larger temperature gradient would lead to stronger storms, reflected by a larger ω_{std} in the midlatitudes. The mean circulation in the Ferrel cell (represented by ω_{500}) will likely also increase due to continuity and the increased momentum carried by the storms. In the tropics, the Held-Hou model (Held & Hou, 1980) establishes a proportionality between the strength of the Hadley circulation ω_{500} and gradients in potential temperature, which in first approximation can be taken as the surface temperature. We have noticed that in the tropics the spatial structure of ω_{500} and ω_{std} are very similar, but why this is the case is not obvious.

The estimated cloud top entrainment index CTE is harder to express in terms of temperatures. Measures like CTE (or EIS or the Lower Stratospheric Stability) capture the temperature inversion magnitude between the boundary layer and surface (Wood & Bretherton, 2006). In the tropical subsidence regions, this inversion strength can be conceptually tied to temperature gradient between the warm equator and colder ocean of subtropics as follows: The free tropospheric temperature is, to a first approximation, homogenized by gravity waves to the value in the convecting regions (weak temperature gradient approximation (Sobel et al., 2001)). Surface temperature in the tropical subsidence regions however reflects the colder ocean temperature. The connection of EIS with the underlying ocean temperature in the case of midlatitudes is less clear. Conceptually, a temperature inversion can occur in cyclonic storms due to kinematic (or alternatively, mechanical) reasons: warm air masses from the midlatitudes are forced on top of the cold polar fronts, creating a temperature inversion scenario. However, more research on the subject is necessary to make more concrete claims.

Given these considerations, it seems that a promising way to express these predictors (and hence cloudiness) in an energy balance model is via the equator-to-pole temperature gradient. Future research should focus on validating this claim in more detail, but also make the qualitative connections we drew here quantitative by providing clear functional forms that connect, e.g., mean ω_{500} or ω_{std} with equator-to-pole temperature gradient.

References

Bony, S., Lau, K.-M., & Sud, Y. C. (1997). Sea surface temperature and large-scale circulation influences on tropical greenhouse effect and cloud radiative forcing. *Journal of Climate*, *10*(8), 2055 - 2077. Retrieved from `https://journals.ametsoc.org/view/journals/clim/10/8/1520-0442_1997_010_2055_sstals_2.0.co_2.xml` doi: 10.1175/1520-0442(1997)010⟨2055:SSTALS⟩2.0.CO;2

Brueck, M., Nuijens, L., & Stevens, B. (2015, March). On the seasonal and synoptic time-scale variability of the north atlantic trade wind region and its low-level clouds. *Journal of the Atmospheric Sciences*, *72*(4), 1428–1446. Retrieved from `https://doi.org/10.1175/jas-d-14-0054.1` doi: 10.1175/jas-d-14-0054.1

Charney, J. G. (1947, oct). The dynamics of long waves in a baroclinic westerly current. *Journal of the Atmospheric Sciences*, *4*(5), 136–162. Retrieved from `http://journals.ametsoc.org/doi/10.1175/1520-0469(1947)004%3C0136:TDOLWI%3E2.0.CO;2` doi: 10.1175/1520-0469(1947)004⟨0136:TDOLWI⟩2.0.CO;2

Datseris, G., & Stevens, B. (2021, August). Earth's albedo and its symmetry. *AGU Advances*, *2*(3). Retrieved from `https://doi.org/10.1029/2021av000440` doi: 10.1029/2021av000440

Eady, E. T. (1949). Long waves and cyclone waves. *Tellus*, *1*(3), 33–52.

Grise, K. M., & Kelleher, M. K. (2021). Midlatitude cloud radiative effect sensitivity to cloud controlling factors in observations and models: Relationship with southern hemisphere jet shifts and climate sensitivity. *Journal of Climate*, *34*(14), 5869–5886. doi: 10.1175/JCLI-D-20-0986.1

Held, I. M., & Hou, A. Y. (1980, March). Nonlinear axially symmetric circulations in a nearly inviscid atmosphere. *Journal of the Atmospheric Sciences*, *37*(3), 515–533. Retrieved from `https://doi.org/10.1175/1520-0469(1980)037<0515:nascia>2.0.co;2` doi: 10.1175/1520-0469(1980)037⟨0515:nascia⟩2.0.co;2

Kawai, H., Koshiro, T., & Webb, M. J. (2017, November). Interpretation of factors controlling low cloud cover and low cloud feedback using a unified predictive index. *Journal of Climate*, *30*(22), 9119–9131. Retrieved from https://doi.org/10.1175/jcli-d-16-0825.1 doi: 10.1175/jcli-d-16-0825.1

Klein, S. A., Hall, A., Norris, J. R., & Pincus, R. (2017). Low-Cloud Feedbacks from Cloud-Controlling Factors: A Review. *Surveys in Geophysics*, *38*(6), 1307–1329. doi: 10.1007/s10712-017-9433-3

Loeb, N. G., Doelling, D. R., Wang, H., Su, W., Nguyen, C., Corbett, J. G., ... Kato, S. (2018, January). Clouds and the earth's radiant energy system (CERES) energy balanced and filled (EBAF) top-of-atmosphere (TOA) edition-4.0 data product. *Journal of Climate*, *31*(2), 895–918. Retrieved from https://doi.org/10.1175/jcli-d-17-0208.1 doi: 10.1175/jcli-d-17-0208.1

Myers, T. A., & Norris, J. R. (2016, March). Reducing the uncertainty in subtropical cloud feedback. *Geophysical Research Letters*, *43*(5), 2144–2148. Retrieved from https://doi.org/10.1002/2015gl067416 doi: 10.1002/2015gl067416

Myers, T. A., Scott, R. C., Zelinka, M. D., Klein, S. A., Norris, J. R., & Caldwell, P. M. (2021). Observational constraints on low cloud feedback reduce uncertainty of climate sensitivity. *Nature Climate Change*, *11*(6), 501–507. Retrieved from http://dx.doi.org/10.1038/s41558-021-01039-0 doi: 10.1038/s41558-021-01039-0

Norris, J. R., & Iacobellis, S. F. (2005, November). North pacific cloud feedbacks inferred from synoptic-scale dynamic and thermodynamic relationships. *Journal of Climate*, *18*(22), 4862–4878. Retrieved from https://doi.org/10.1175/jcli3558.1 doi: 10.1175/jcli3558.1

Pierrehumbert, & Swanson. (1995, jan). Baroclinic Instability. *Annual Review of Fluid Mechanics*, *27*(1), 419–467. Retrieved from http://fluid.annualreviews.org/cgi/doi/10.1146/annurev.fluid.27.1.419 doi: 10.1146/annurev.fluid.27.1.419

Qu, X., Hall, A., Klein, S. A., & DeAngelis, A. M. (2015, September). Positive tropical marine low-cloud cover feedback inferred from cloud-controlling factors. *Geophysical Research Letters*, *42*(18), 7767–7775. Retrieved from https://doi.org/10.1002/2015gl065627 doi: 10.1002/2015gl065627

Sobel, A. H., Nilsson, J., & Polvani, L. M. (2001). The weak temperature gradient approximation and balanced tropical moisture waves. *Journal of the Atmospheric Sciences*, *58*(23), 3650–3665. doi: 10.1175/1520-0469(2001)058⟨3650:TWTGAA⟩2.0.CO;2

Stephens, G. L., O'Brien, D., Webster, P. J., Pilewski, P., Kato, S., & Li, J.-l. (2015, mar). The albedo of Earth. *Reviews of Geophysics*, *53*(1), 141–163. Retrieved from http://doi.wiley.com/10.1002/2014RG000449 doi: 10.1002/2014RG000449

Stevens, B., & Brenguier, J.-L. (2009). Cloud-controlling factors: low clouds. In J. Heintzenberg & R. J. Charlson (Eds.), *Clouds in the perturbed climate system* (chap. 8). The MIT Press. Retrieved from https://doi.org/10.7551/mitpress/9780262012874.001.0001 doi: 10.7551/mitpress/9780262012874.001.0001

Stevens, B., & Schwartz, S. E. (2012, May). Observing and modeling earth's energy flows. *Surveys in Geophysics*, *33*(3-4), 779–816. Retrieved from https://doi.org/10.1007/s10712-012-9184-0 doi: 10.1007/s10712-012-9184-0

Wood, R., & Bretherton, C. S. (2006). On the relationship between stratiform low cloud cover and lower-tropospheric stability. *Journal of Climate*, *19*(24), 6425–6432. doi: 10.1175/JCLI3988.1